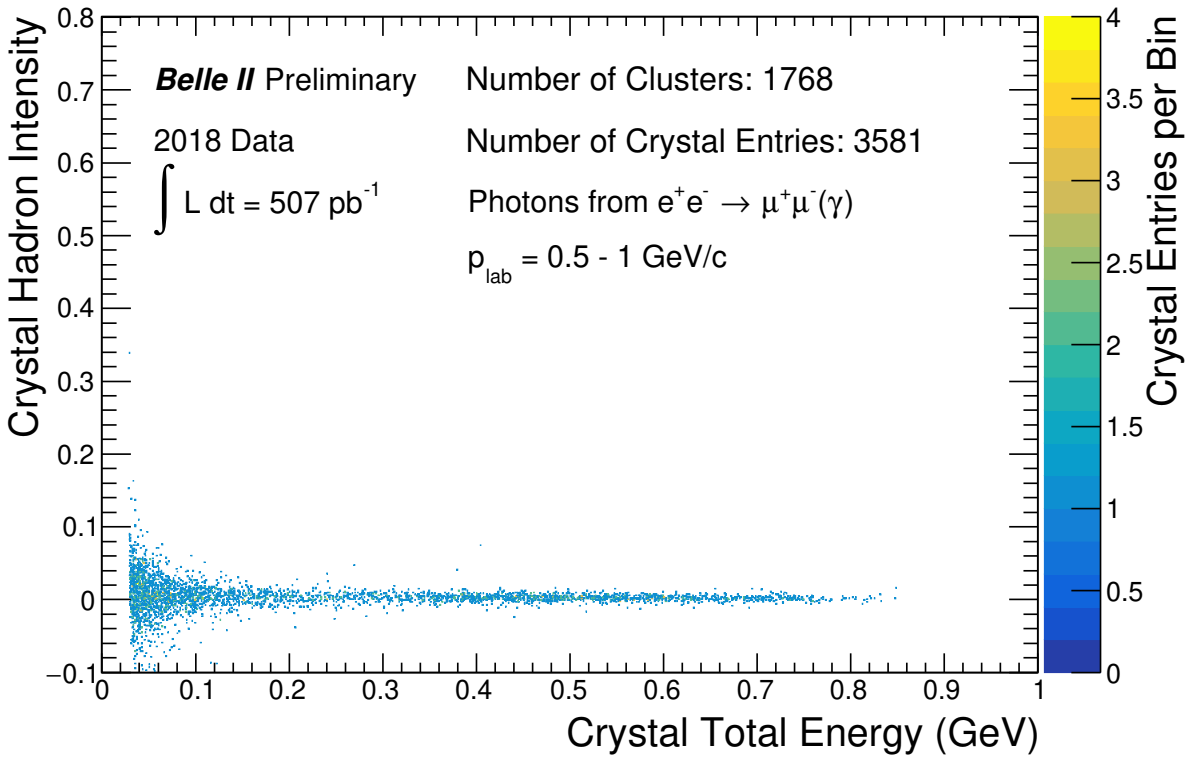

Figure 1: Crystal hadron intensity vs crystal total energy for CsI(Tl) crystals in calorimeter clusters produced by photons in Phase 2 Data in the momentum range 0.5-1 GeV/c. Photons are selected from $e^+e^- \to \mu^+\mu^-(\gamma)$ control sample. For further discussion on the result see Section 4 in reference [1]. For selection details see Appendix D in reference [2].

Figure citations:

[1] S. Longo and J. M. Roney, *Kaon-long and Photon Identification in Phase 2 Data and MC using Pulse Shape Discrimination* (BELLE2-NOTE-TE-2019-015), 2019.

[2] S. Longo and J. M. Roney, *Studies of Charged Particle Interactions in CsI(Tl) using Calorimeter Pulse Shape Discrimination* (BELLE2-NOTE-TE-2019-012), 2019.

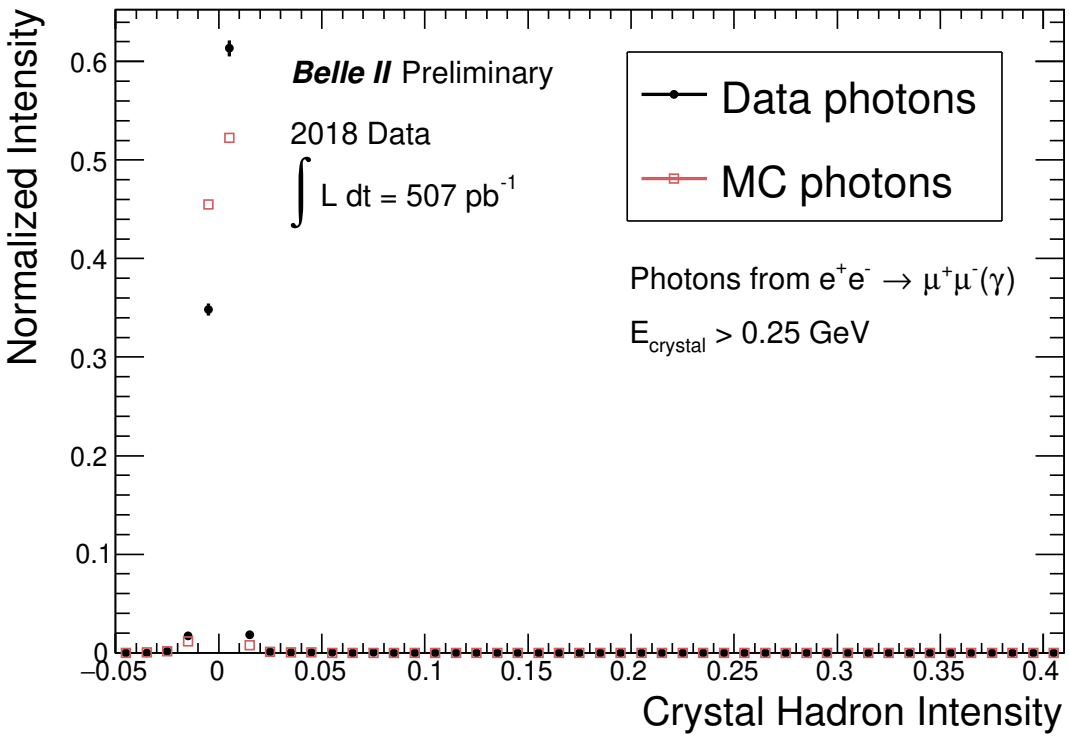

Figure 2: Histogram of the crystal hadron intensity for CsI(Tl) crystals with energy above 0.25 GeV in calorimeter clusters produced by photons selected from $e^+e^- \to \mu^+\mu^-(\gamma)$ control sample in Phase 2 Data and MC. Errors are statistical only. For further discussion on the result see Section 4 of reference [1]. For selection details see Appendix D in reference [2].

Figure citations:

[1] S. Longo and J. M. Roney, *Kaon-long and Photon Identification in Phase 2 Data and MC using Pulse Shape Discrimination* (BELLE2-NOTE-TE-2019-015), 2019.

[2] S. Longo and J. M. Roney, *Studies of Charged Particle Interactions in CsI(Tl) using Calorimeter Pulse Shape Discrimination* (BELLE2-NOTE-TE-2019-012), 2019.

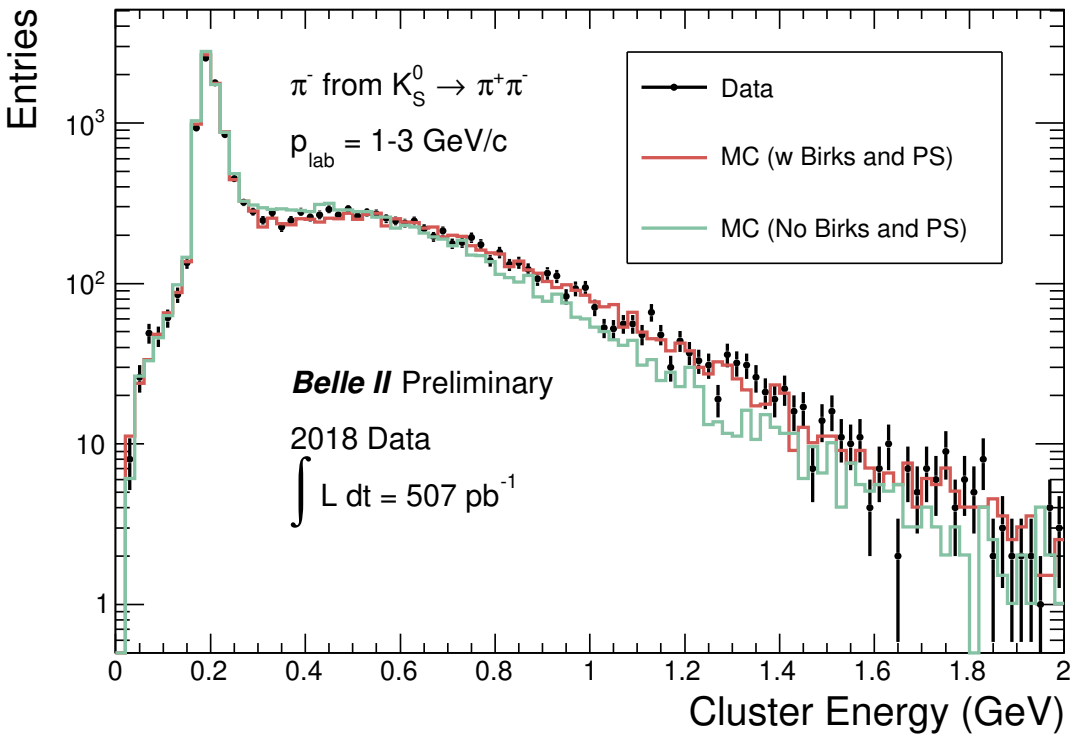

Figure 3: Cluster energy distribution of π^- with $p_{\rm lab} = 1 - 3$ GeV/c, selected from $K^0_S \to \pi^+\pi^-$ control sample from Phase 2 Data and Monte Carlo (MC). MC labelled "No Birks and PS" does not include simulations of CsI(Tl) scintillation response to highly ionizing particles. MC labelled "w Birks and PS" includes simulations of the Birks scintillation efficiency and simulations of the ionization dE/dx dependent CsI(Tl) scintillation pulse shapes. Errors are statistical only. For further discussion on the result see Section 7 of reference below. For selection details see Appendix E in reference below.

Figure citation:

S. Longo and J. M. Roney, *Studies of Charged Particle Interactions in CsI(Tl) using Calorimeter Pulse Shape Discrimination* (BELLE2-NOTE-TE-2019-012), 2019.

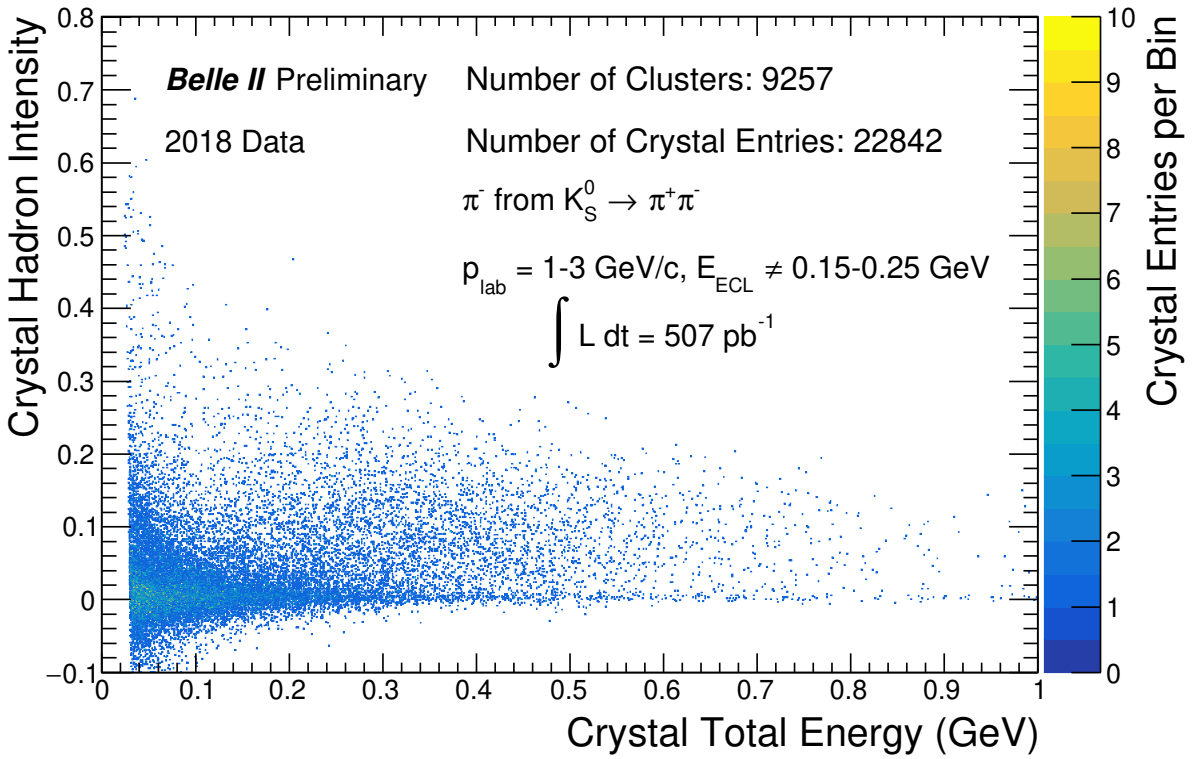

Figure 4: Crystal hadron intensity vs crystal total energy for CsI(Tl) crystals in calorimeter clusters produced by π^- in Phase 2 Data with $p_{\text{lab}} = 1 - 3$ GeV/c and cluster energy outside the range $0.15 - 0.25$ GeV (ionization cluster veto to select hadronic showers). π^- are selected from $K^0_S \to \pi^+\pi^-$ control sample. For further discussion on the result see Section 7 of reference below. For selection details see Appendix E in reference below.

Figure citation:

S. Longo and J. M. Roney, *Studies of Charged Particle Interactions in CsI(Tl) using Calorimeter Pulse Shape Discrimination* (BELLE2-NOTE-TE-2019-012), 2019.

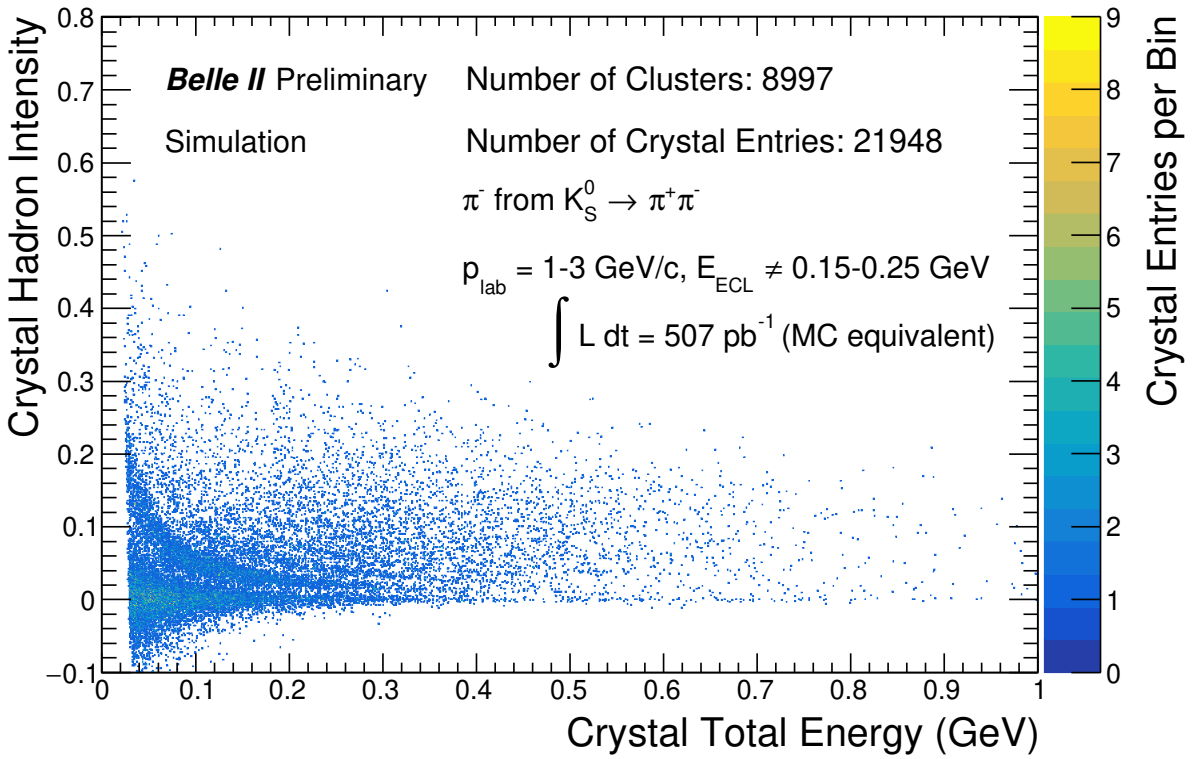

Figure 5: Crystal hadron intensity vs crystal total energy for CsI(Tl) crystals in calorimeter clusters produced by π^- in Phase 2 simulation with $p_{\text{lab}} = 1 - 3$ GeV/c and cluster energy outside the range $0.15 - 0.25$ GeV (ionization cluster veto to select hadronic showers). π^- are selected from $K^0_S \to \pi^+\pi^-$ control sample. For further discussion on the result see Section 7 of reference below. For selection details see Appendix E in reference below.

Figure citation:

S. Longo and J. M. Roney, *Studies of Charged Particle Interactions in CsI(Tl) using Calorimeter Pulse Shape Discrimination* (BELLE2-NOTE-TE-2019-012), 2019.

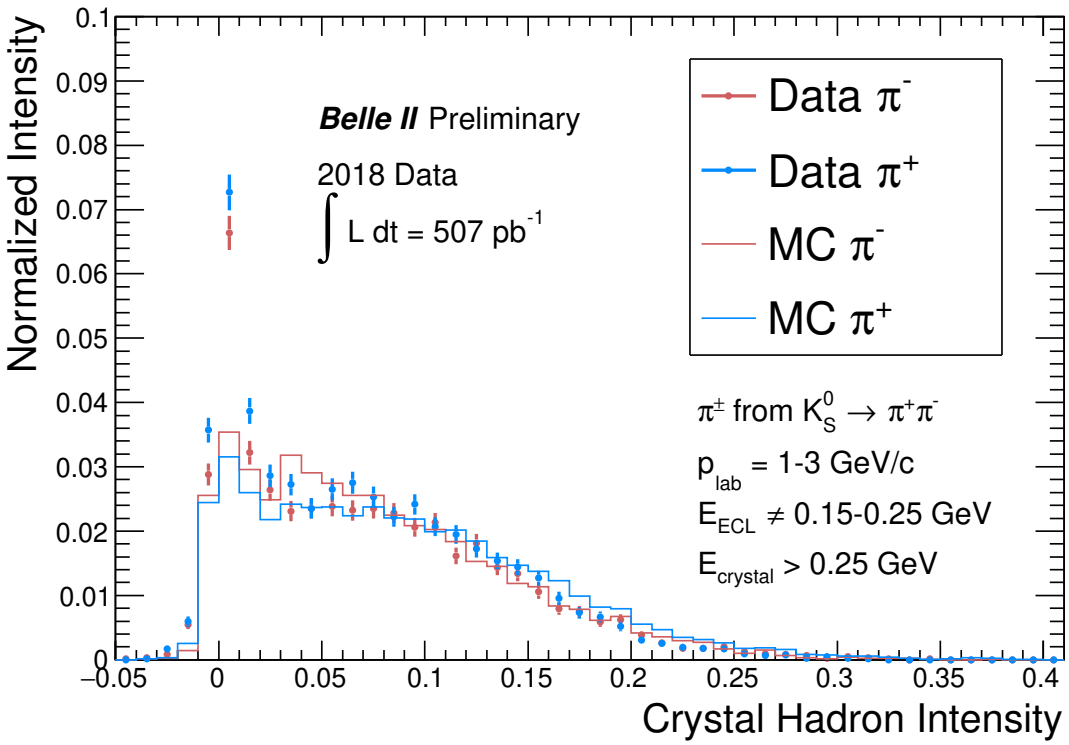

Figure 6: Histogram of the crystal hadron intensity for CsI(Tl) crystals with energy above 0.25 GeV, in calorimeter clusters produced by π^- with $p_{\rm lab} = 1-3$ GeV/c and cluster energy outside the range $0.15-0.25$ GeV (ionization cluster veto to select hadronic showers). π^+ are selected from $K^0_S \to \pi^+\pi^-$ control sample. Errors are statistical only. For further discussion on the result see Section 7 of reference below. For selection details see Appendix E in reference below.

Figure citation:

S. Longo and J. M. Roney, *Studies of Charged Particle Interactions in CsI(Tl) using Calorimeter Pulse Shape Discrimination* (BELLE2-NOTE-TE-2019-012), 2019.

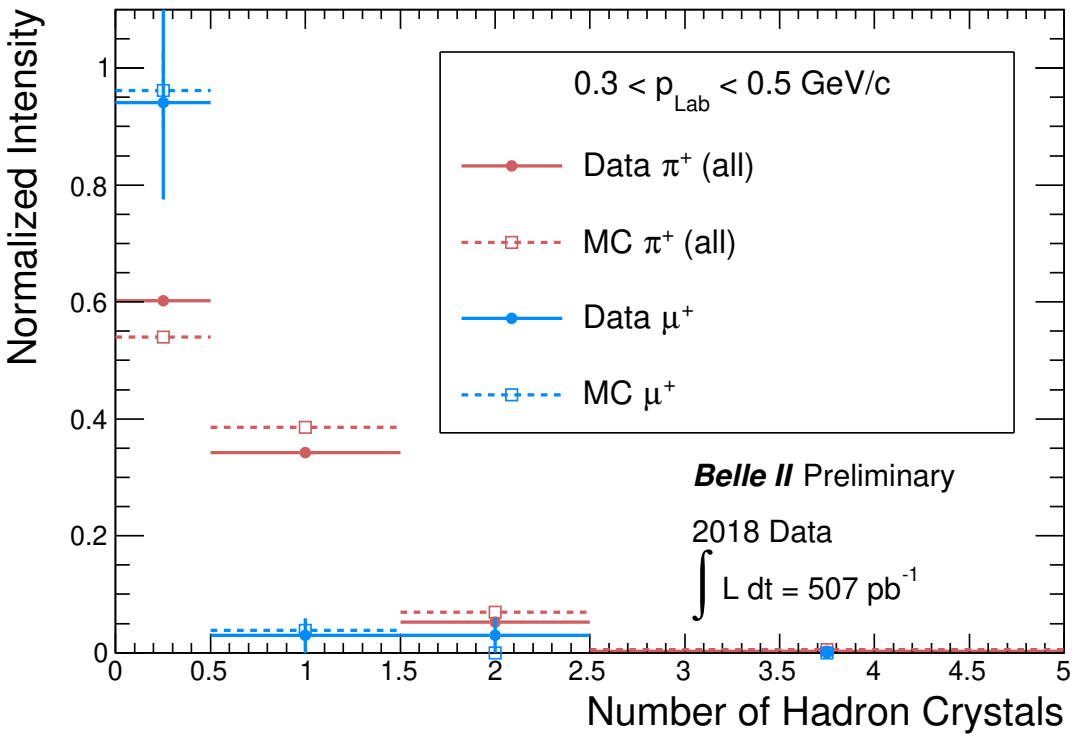

Figure 7: Distribution of "Number of Hadron Crystals" defined as the sum of the cluster association weights of crystals in a calorimeter cluster that have a significant amount of hadron scintillation component emission. π^+ are selected from $K^0_S \to \pi^+\pi^-$ control sample and μ^- are selected from $e^+e^- \to \mu^+\mu^-(\gamma)$ control sample from Phase 2 Data and MC. Errors are statistical only. For further discussion on the result see Section 10 of reference below.

Figure citation:

S. Longo and J. M. Roney, *Studies of Charged Particle Interactions in CsI(Tl) using Calorimeter Pulse Shape Discrimination* (BELLE2-NOTE-TE-2019-012), 2019.

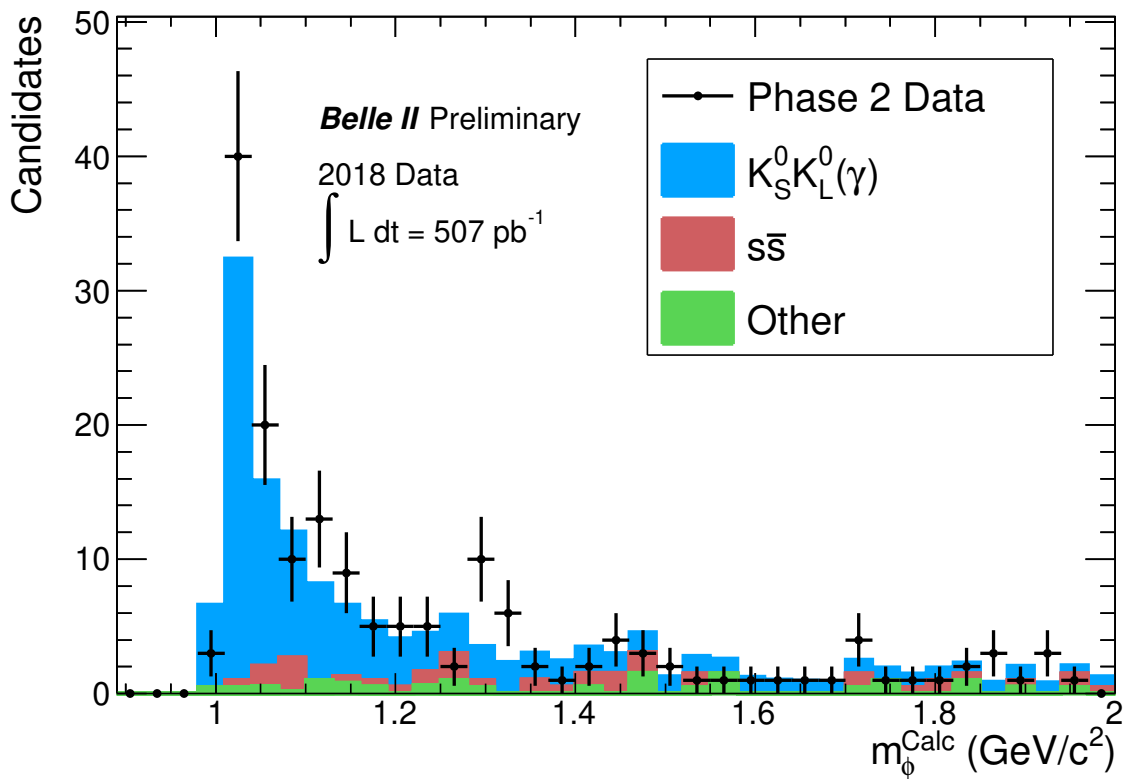

Figure 8: Distribution of the invariant mass computed using the K_S^0 and K_L^0 candidates selected from $e^+e^- \to \phi\gamma \to K_S^0K_L^0\gamma$ control sample from Phase 2 Data and MC. The K_L^0 momentum magnitude is computed from γ and K_S^0 candidates by applying total energy conservation. The K_L^0 momentum direction is given by the location of the candidate calorimeter cluster. K_L^0 candidates in the region $m_\phi^{\text{Calc}} < 1.12$ GeV/c^2 are selected. Errors are statistical only. For further discussion on the result and selection details see appendix of reference below.

Figure citation:

S. Longo and J. M. Roney, *Kaon-long and Photon Identification in Phase 2 Data and MC using Pulse Shape Discrimination* (BELLE2-NOTE-TE-2019-015), 2019.

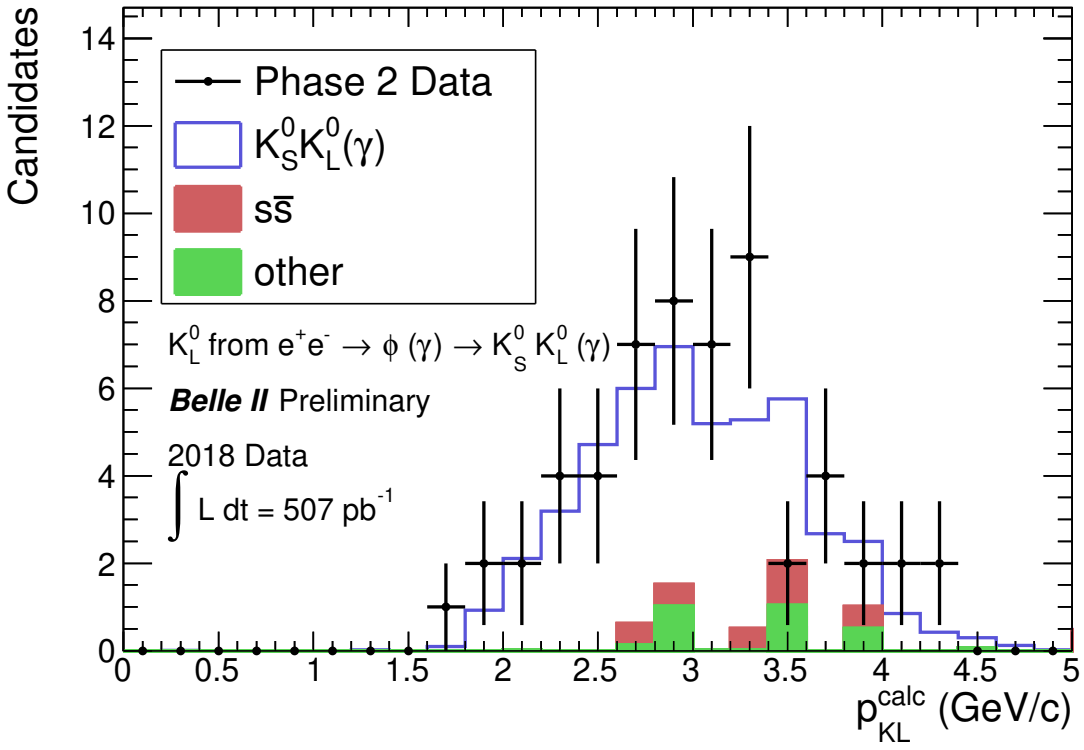

Figure 9: Distribution of calculated momentum magnitude for K^0_L candidates from $e^+e^- \to \phi\gamma \to K^0_S K^0_L \gamma$ control sample selected from Phase 2 Data and MC. Errors are statistical only. For further discussion on the result and selection details see appendix of reference below.

Figure citation:

S. Longo and J. M. Roney, *Kaon-long and Photon Identification in Phase 2 Data and MC using Pulse Shape Discrimination* (BELLE2-NOTE-TE-2019-015), 2019.

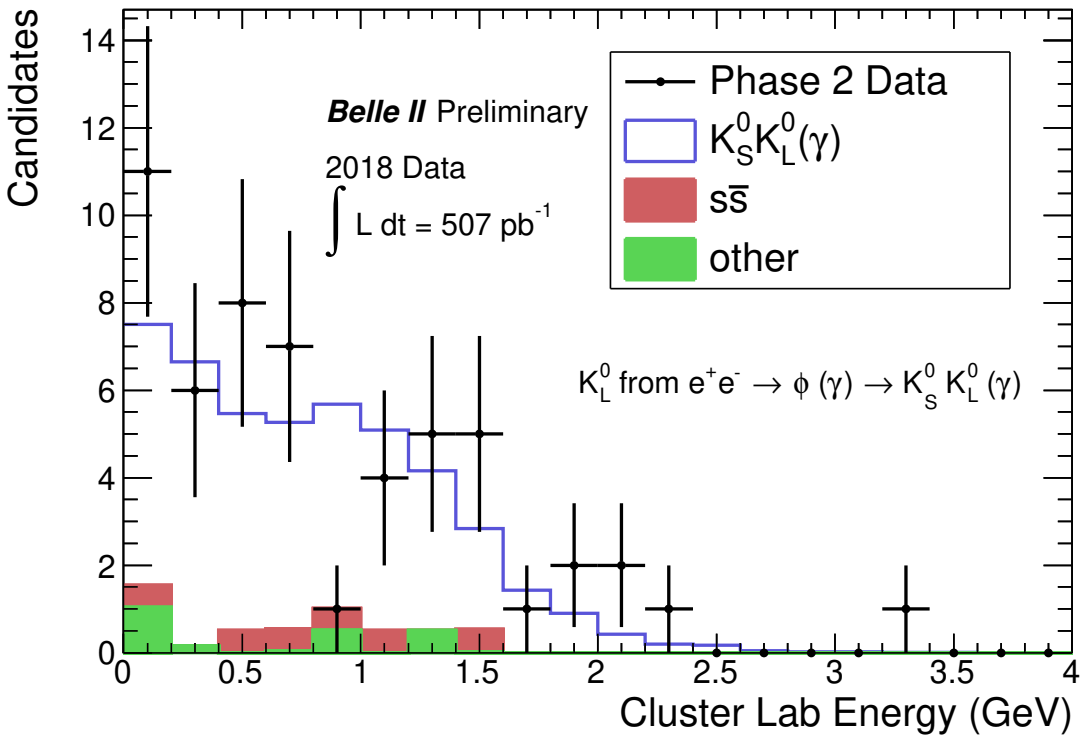

Figure 10: Distribution of measured cluster energy for K_L^0 candidates from $e^+e^- \to \phi\gamma \to K_S^0 K_L^0 \gamma$ control sample selected from Phase 2 Data and MC. Errors are statistical only. For further discussion on the result and selection details see appendix of reference below.

Figure citation:

S. Longo and J. M. Roney, *Kaon-long and Photon Identification in Phase 2 Data and MC using Pulse Shape Discrimination* (BELLE2-NOTE-TE-2019-015), 2019.

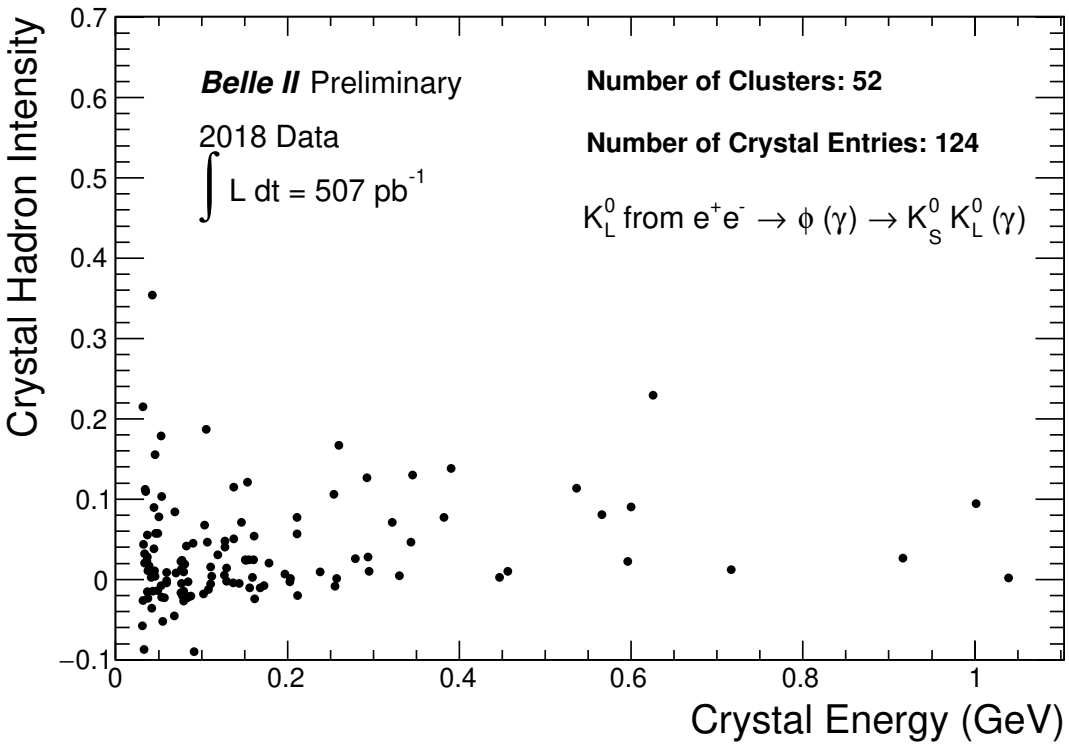

Figure 11: Crystal hadron intensity vs crystal total energy for CsI(Tl) crystals in calorimeter clusters produced by K_L^0 selected from $e^+e^- \to \phi\gamma \to K_S^0 K_L^0 \gamma$ control sample in Phase 2 Data. For further discussion on the result see Section 4 in reference below. For selection details see appendix in reference below.

Figure citation:

S. Longo and J. M. Roney, *Kaon-long and Photon Identification in Phase 2 Data and MC using Pulse Shape Discrimination* (BELLE2-NOTE-TE-2019-015), 2019.

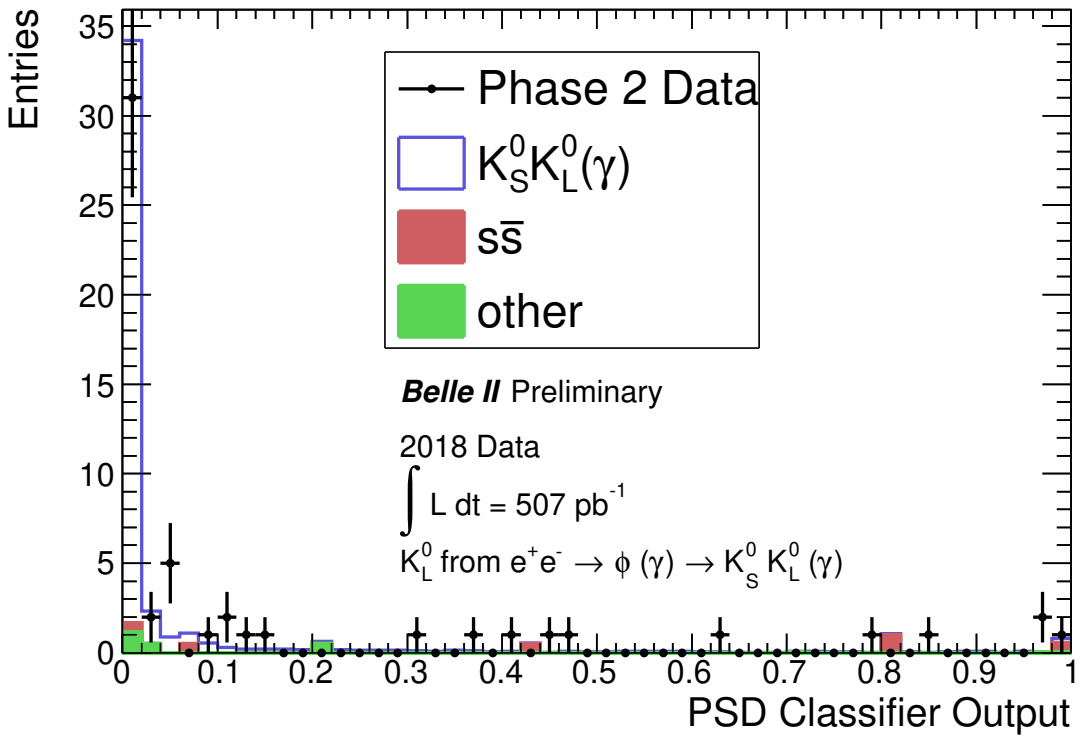

Figure 12: Distribution of pulse shape discrimination based multivariate classifier output for calorimeter clusters produced by K^0_L candidates selected from $e^+e^- \to \phi\gamma \to K^0_S K^0_L \gamma$ control sample in Phase 2 Data and MC. Errors are statistical only. For further discussion on the result see Section 4 in reference below. For selection details see appendix in reference below.

Figure citation:

S. Longo and J. M. Roney, *Kaon-long and Photon Identification in Phase 2 Data and MC using Pulse Shape Discrimination* (BELLE2-NOTE-TE-2019-015), 2019.

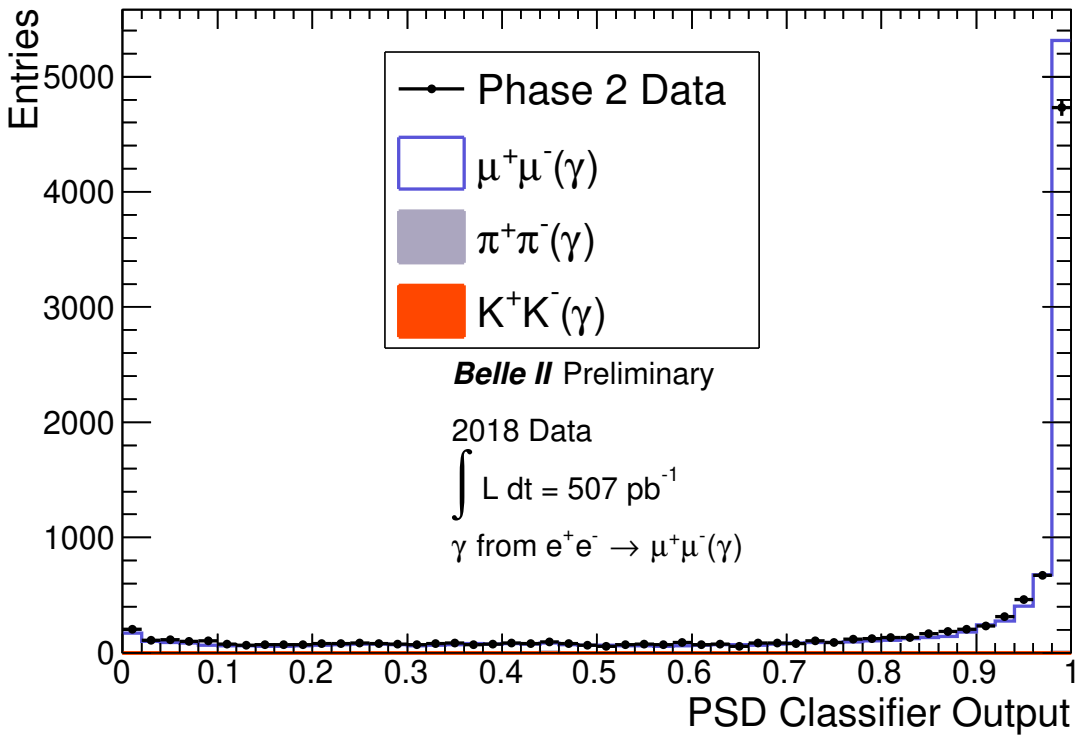

Figure 13: Distribution of pulse shape discrimination based multivariate classifier output for calorimeter clusters produced by photons candidates selected from $e^+e^- \to \mu^+\mu^-(\gamma)$ control sample in Phase 2 Data and MC. Errors are statistical only. For further discussion on the result see Section 4 in reference [1]. For selection details see Appendix D in reference [2].

Figure citations:

[1] S. Longo and J. M. Roney, *Kaon-long and Photon Identification in Phase 2 Data and MC using Pulse Shape Discrimination* (BELLE2-NOTE-TE-2019-015), 2019.

[2] S. Longo and J. M. Roney, *Studies of Charged Particle Interactions in CsI(Tl) using Calorimeter Pulse Shape Discrimination* (BELLE2-NOTE-TE-2019-012), 2019.

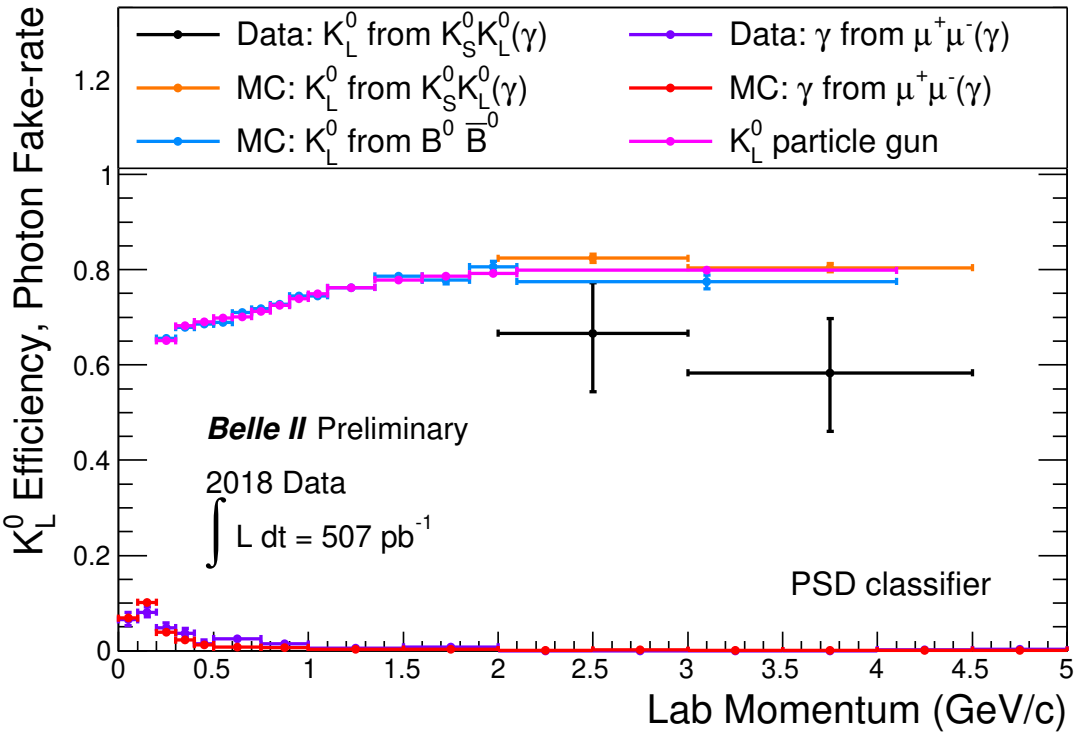

Figure 14: K_L^0 identification efficiency and photon fake-rate (*photon-as-hadron*) as a function of momentum for pulse shape discrimination based multivariate classifier for tight cut of $\Theta_{\mathrm{PSD}} < 0.02$, where Θ_{PSD} is the output of the classifier. Errors are statistical only. For further discussion on the result see Section 4 in reference below.

Figure citation:

S. Longo and J. M. Roney, *Kaon-long and Photon Identification in Phase 2 Data and MC using Pulse Shape Discrimination* (BELLE2-NOTE-TE-2019-015), 2019.

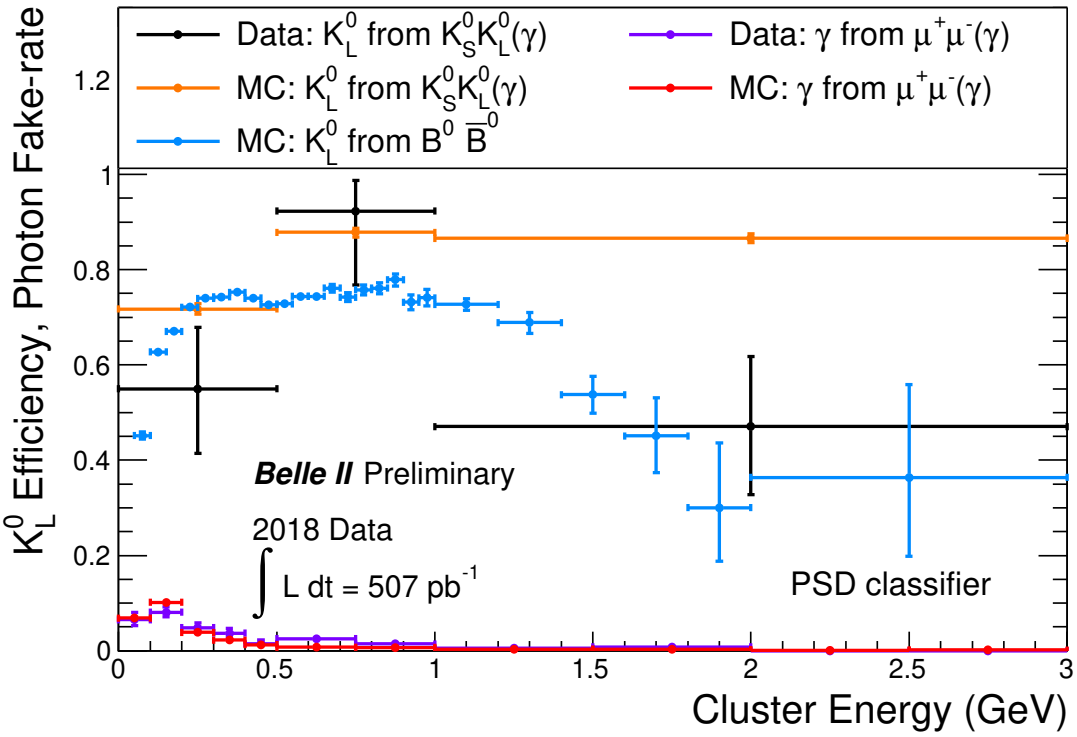

Figure 15: K^0_L identification efficiency and photon fake-rate (*photon-as-hadron*) as a function of cluster energy for pulse shape discrimination based multivariate classifier for tight cut of $\Theta_{\rm PSD} < 0.02$, where $\Theta_{\rm PSD}$ is the output of the classifier. Errors are statistical only. For further discussion on the result see Section 4 in reference below.

Figure citation:

S. Longo and J. M. Roney, *Kaon-long and Photon Identification in Phase 2 Data and MC using Pulse Shape Discrimination* (BELLE2-NOTE-TE-2019-015), 2019.

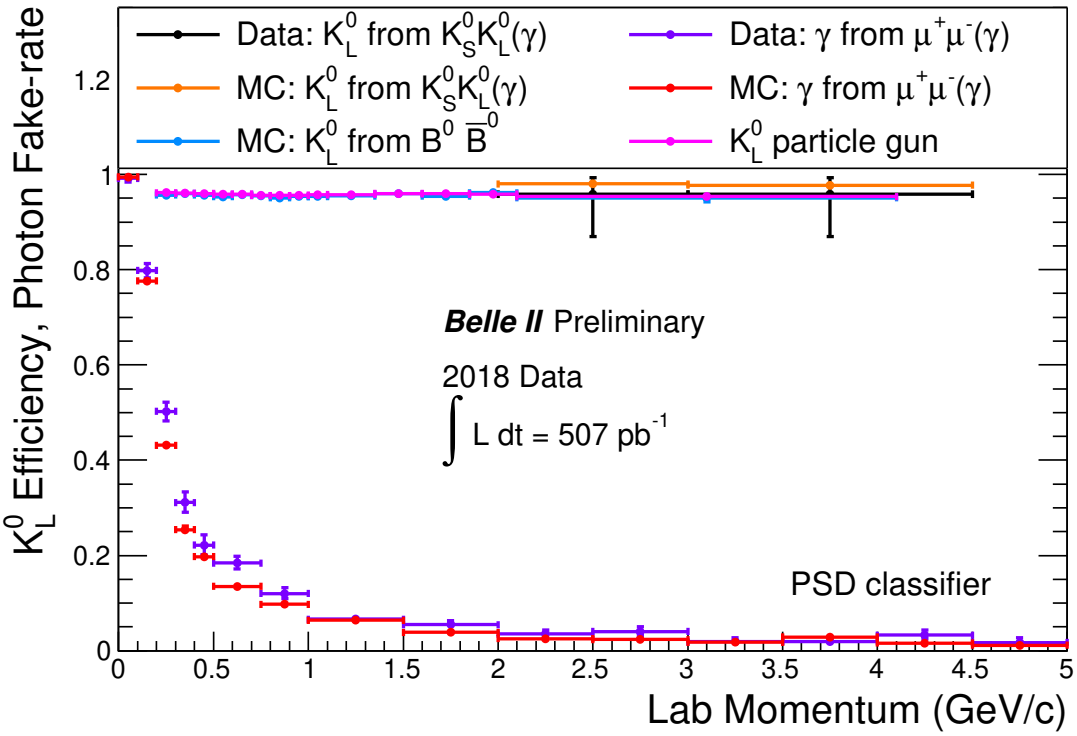

Figure 16: K^0_L identification efficiency and photon fake-rate (*photon-as-hadron*) as a function of momentum for pulse shape discrimination based multivariate classifier for loose cut to achieve 95% efficiency for K^0_L identification. Errors are statistical only. For further discussion on the result see Section 4 in reference below.

Figure citation:

S. Longo and J. M. Roney, *Kaon-long and Photon Identification in Phase 2 Data and MC using Pulse Shape Discrimination* (BELLE2-NOTE-TE-2019-015), 2019.

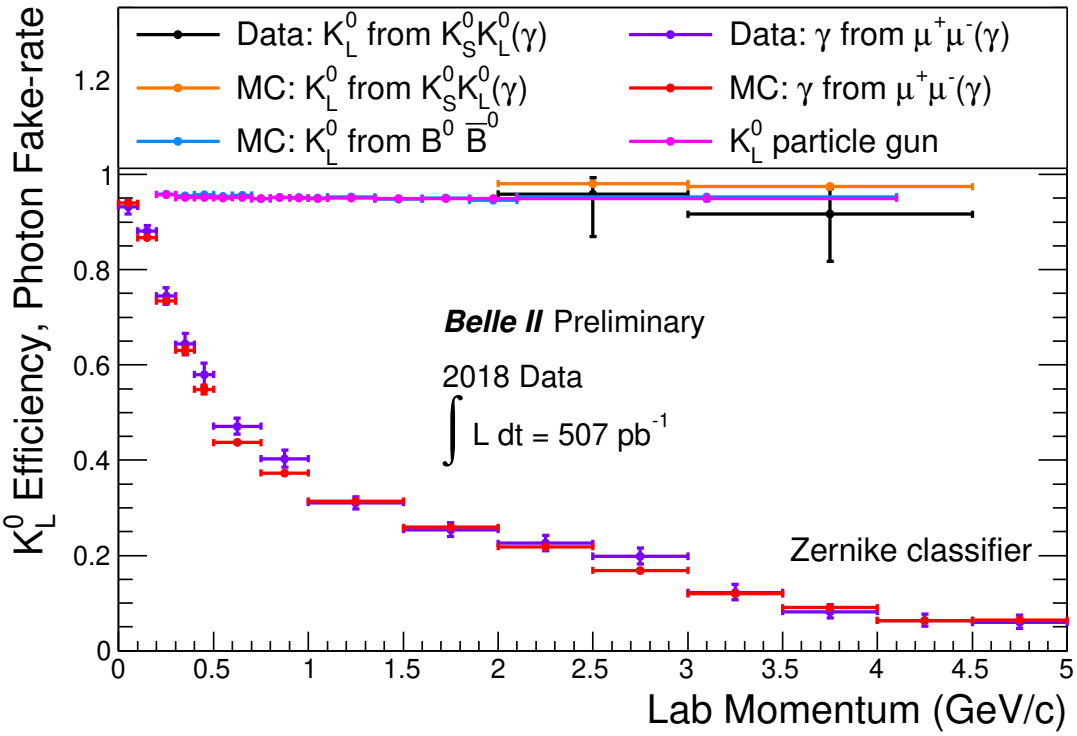

Figure 17: K^0_L identification efficiency and photon fake-rate (*photon-as-hadron*) as a function of momentum for shower shape based multivariate classifier for loose cut to achieve 95% efficiency for K^0_L identification. Errors are statistical only. For further discussion on the result see Section 4 in reference below.

Figure citation:

S. Longo and J. M. Roney, *Kaon-long and Photon Identification in Phase 2 Data and MC using Pulse Shape Discrimination* (BELLE2-NOTE-TE-2019-015), 2019.